

Photon-hadron jet correlations in $p + p$ and Au + Au collisions at $\sqrt{s_{NN}} = 200$ GeV

A. Adare,¹¹ S. Afanasiev,²⁵ C. Aidala,^{12,37} N. N. Ajitanand,⁵⁴ Y. Akiba,^{48,49} H. Al-Bataineh,⁴³ J. Alexander,⁵⁴ A. Al-Jamel,⁴³ K. Aoki,^{31,48} L. Aphecetche,⁵⁶ R. Armendariz,⁴³ S. H. Aronson,⁶ J. Asai,^{48,49} E. T. Atomssa,³² R. Averbeck,⁵⁵ T. C. Awes,⁴⁴ B. Azmoun,⁶ V. Babintsev,²¹ M. Bai,⁵ G. Baksay,¹⁷ L. Baksay,¹⁷ A. Baldisseri,¹⁴ K. N. Barish,⁷ P. D. Barnes,³⁴ B. Bassalleck,⁴² A. T. Basye,¹ S. Bathe,⁷ S. Batsouli,^{12,44} V. Baublis,⁴⁷ F. Bauer,⁷ C. Baumann,³⁸ A. Bazilevsky,⁶ S. Belikov,^{6,24,*} R. Bennett,⁵⁵ A. Berdnikov,⁵¹ Y. Berdnikov,⁵¹ A. A. Bickley,¹¹ M. T. Bjornald,¹² J. G. Boissevain,³⁴ H. Borel,¹⁴ K. Boyle,⁵⁵ M. L. Brooks,³⁴ D. S. Brown,⁴³ D. Bucher,³⁸ H. Buesching,⁶ V. Bumazhnov,²¹ G. Bunce,^{6,49} J. M. Burward-Hoy,³⁴ S. Butsyk,^{34,55} C. M. Camacho,³⁴ S. Campbell,⁵⁵ J.-S. Chai,²⁶ B. S. Chang,⁶³ W. C. Chang,² J.-L. Charvet,¹⁴ C.-H. Chen,⁵⁵ S. Chernichenko,²¹ J. Chiba,²⁷ C. Y. Chi,¹² M. Chiu,^{12,22} I. J. Choi,⁶³ R. K. Choudhury,⁴ T. Chujo,^{59,60} P. Chung,⁵⁴ A. Churnin,²¹ V. Cianciolo,⁴⁴ Z. Citron,⁵⁵ C. R. Clevén,¹⁹ Y. Cobigo,¹⁴ B. A. Cole,¹² M. P. Comets,⁴⁵ M. Connors,⁵⁵ P. Constantin,^{24,34} M. Csanád,¹⁶ T. Csörgő,²⁸ T. Dahms,⁵⁵ S. Dairaku,^{31,48} K. Das,¹⁸ G. David,⁶ M. B. Deaton,¹ K. Dehmelt,¹⁷ H. Delagrange,⁵⁶ A. Denisov,²¹ D. d'Enterria,^{12,32} A. Deshpande,^{49,55} E. J. Desmond,⁶ O. Dietzsch,⁵² A. Dion,⁵⁵ M. Donadelli,⁵² J. L. Drachenberg,¹ O. Drapier,³² A. Drees,⁵⁵ K. A. Drees,⁵ A. K. Dubey,⁶² A. Durum,²¹ D. Dutta,⁴ V. Dzhordzhadze,^{7,57} Y. V. Efremenko,⁴⁴ J. Egdemir,⁵⁵ F. Ellinghaus,¹¹ W. S. Emam,⁷ T. Engelmöre,¹² A. Enokizono,^{20,33} H. En'yo,^{48,49} B. Espagnon,⁴⁵ S. Esumi,⁵⁹ K. O. Eyster,⁷ B. Fadem,³⁹ D. E. Fields,^{42,49} M. Finger Jr.,^{8,25} M. Finger,^{8,25} F. Fleuret,³² S. L. Fokin,³⁰ B. Forestier,³⁵ Z. Fraenkel,^{62,*} J. E. Frantz,^{12,55} A. Franz,⁶ A. D. Frawley,¹⁸ K. Fujiwara,⁴⁸ Y. Fukao,^{31,48} S.-Y. Fung,⁷ T. Fusayasu,⁴¹ S. Gadrat,³⁵ I. Garishvili,⁵⁷ F. Gastineau,⁵⁶ M. Germain,⁵⁶ A. Glenn,^{11,57} H. Gong,⁵⁵ M. Gonin,³² J. Gosset,¹⁴ Y. Goto,^{48,49} R. Granier de Cassagnac,³² N. Grau,^{12,24} S. V. Greene,⁶⁰ M. Grosse Perdekamp,^{22,49} T. Gunji,¹⁰ H.-Å. Gustafsson,³⁶ T. Hachiya,^{20,48} A. Hadj Henni,⁵⁶ C. Haegemann,⁴² J. S. Haggerty,⁶ M. N. Hagiwara,¹ H. Hamagaki,¹⁰ R. Han,⁴⁶ H. Harada,²⁰ E. P. Hartouni,³³ K. Haruna,²⁰ M. Harvey,⁶ E. Haslum,³⁶ K. Hasuko,⁴⁸ R. Hayano,¹⁰ M. Heffner,³³ T. K. Hemmick,⁵⁵ T. Hester,⁷ J. M. Heuser,⁴⁸ X. He,¹⁹ H. Hiejima,²² J. C. Hill,²⁴ R. Hobbs,⁴² M. Hohmann,¹⁷ M. Holmes,⁶⁰ W. Holzmann,⁵⁴ K. Homma,²⁰ B. Hong,²⁹ T. Horaguchi,^{10,48,58} D. Hornback,⁵⁷ S. Huang,⁶⁰ M. G. Hur,²⁶ T. Ichihara,^{48,49} R. Ichimiya,⁴⁸ Y. Ikeda,⁵⁹ K. Imai,^{31,48} J. Imrek,¹⁵ M. Inaba,⁵⁹ Y. Inoue,^{48,50} D. Isenhower,¹ L. Isenhower,¹ M. Ishihara,⁴⁸ T. Isobe,¹⁰ M. Issah,⁵⁴ A. Isupov,²⁵ D. Ivanischev,⁴⁷ B. V. Jacak,^{55,†} J. Jia,¹² J. Jin,¹² O. Jinnouchi,⁴⁹ B. M. Johnson,⁶ K. S. Joo,⁴⁰ D. Jouan,⁴⁵ F. Kajihara,^{10,48} S. Kametani,^{10,48,61} N. Kamihara,^{48,49,58} J. Kamin,⁵⁵ M. Kaneta,⁴⁹ J. H. Kang,⁶³ H. Kanou,^{48,58} J. Kapustinsky,³⁴ T. Kawagishi,⁵⁹ D. Kawal,^{37,49} A. V. Kazantsev,³⁰ S. Kelly,¹¹ T. Kempel,²⁴ A. Khanzadeev,⁴⁷ K. M. Kijima,²⁰ J. Kikuchi,⁶¹ B. I. Kim,²⁹ D. H. Kim,⁴⁰ D. J. Kim,⁶³ E. Kim,⁵³ S. H. Kim,⁶³ Y.-S. Kim,²⁶ E. Kinney,¹¹ K. Kiriluk,¹¹ A. Kiss,¹⁶ E. Kistenev,⁶ A. Kiyomichi,⁴⁸ J. Klay,³³ C. Klein-Boeing,³⁸ L. Kochenda,⁴⁷ V. Kochetkov,²¹ B. Komkov,⁴⁷ M. Konno,⁵⁹ J. Koster,²² D. Kotchetkov,⁷ A. Kozlov,⁶² A. Král,¹³ A. Kravitz,¹² P. J. Kroon,⁶ J. Kubart,^{8,23} G. J. Kunde,³⁴ N. Kurihara,¹⁰ K. Kurita,^{48,50} M. Kurosawa,⁴⁸ M. J. Kweon,²⁹ Y. Kwon,^{57,63} G. S. Kyle,⁴³ R. Lacey,⁵⁴ Y.-S. Lai,¹² Y. S. Lai,¹² J. G. Lajoie,²⁴ D. Layton,²² A. Lebedev,²⁴ Y. Le Bornec,⁴⁵ S. Leckey,⁵⁵ D. M. Lee,³⁴ K. B. Lee,²⁹ M. K. Lee,⁶³ T. Lee,⁵³ M. J. Leitch,³⁴ M. A. L. Leite,⁵² B. Lenzi,⁵² P. Liebing,⁴⁹ H. Lim,⁵³ T. Liška,¹³ A. Litvinenko,²⁵ H. Liu,⁴³ M. X. Liu,³⁴ X. Li,⁹ X. H. Li,⁷ B. Love,⁶⁰ D. Lynch,⁶ C. F. Maguire,⁶⁰ Y. I. Makdisi,^{5,6} A. Malakhov,²⁵ M. D. Malik,⁴² V. I. Manko,³⁰ E. Mannel,¹² Y. Mao,^{46,48} L. Mašek,^{8,23} H. Masui,⁵⁹ F. Matathias,^{12,55} M. C. McCain,²² M. McCumber,⁵⁵ P. L. McGaughey,³⁴ N. Means,⁵⁵ B. Meredith,²² Y. Miake,⁵⁹ P. Mikeš,^{8,23} K. Miki,⁵⁹ T. E. Miller,⁶⁰ A. Milov,^{6,55} S. Mioduszewski,⁶ G. C. Mishra,¹⁹ M. Mishra,³ J. T. Mitchell,⁶ M. Mitrovski,⁵⁴ A. K. Mohanty,⁴ Y. Morino,¹⁰ A. Morreale,⁷ D. P. Morrison,⁶ J. M. Moss,³⁴ T. V. Moukhanova,³⁰ D. Mukhopadhyay,⁶⁰ J. Murata,^{48,50} S. Nagamiya,²⁷ Y. Nagata,⁵⁹ J. L. Nagle,¹¹ M. Naglis,⁶² M. I. Nagy,¹⁶ I. Nakagawa,^{48,49} Y. Nakamiya,²⁰ T. Nakamura,²⁰ K. Nakano,^{48,58} J. Newby,³³ M. Nguyen,⁵⁵ T. Niita,⁵⁹ B. E. Norman,³⁴ R. Nouicer,⁶ A. S. Nyanin,³⁰ J. Nystrand,³⁶ E. O'Brien,⁶ S. X. Oda,¹⁰ C. A. Ogilvie,²⁴ H. Ohnishi,⁴⁸ I. D. Ojha,⁶⁰ H. Okada,^{31,48} K. Okada,⁴⁹ M. Oka,⁴⁹ O. O. Omiwade,¹ Y. Onuki,⁴⁸ A. Oskarsson,³⁶ I. Otterlund,³⁶ M. Ouchida,²⁰ K. Ozawa,¹⁰ R. Pak,⁶ D. Pal,⁶⁰ A. P. T. Palounek,³⁴ V. Pantuev,⁵⁵ V. Papavassiliou,⁴³ J. Park,⁵³ W. J. Park,²⁹ S. F. Pate,⁴³ H. Pei,²⁴ J.-C. Peng,²² H. Pereira,¹⁴ V. Peresedov,²⁵ D. Yu. Peressounko,³⁰ C. Pinkenburg,⁶ R. P. Pisani,⁶ M. L. Purschke,⁶ A. K. Purwar,^{34,55} H. Qu,¹⁹ J. Rak,^{24,42} A. Rakotozafindrabe,³² I. Ravinovich,⁶² K. F. Read,^{44,57} S. Rembeczki,¹⁷ M. Reuter,⁵⁵ K. Reygers,³⁸ V. Riabov,⁴⁷ Y. Riabov,⁴⁷ D. Roach,⁶⁰ G. Roche,³⁵ S. D. Rolnick,⁷ A. Romana,^{32,*} M. Rosati,²⁴ S. S. E. Rosendahl,³⁶ P. Rosnet,³⁵ P. Rukoyatkin,²⁵ P. Ružička,²³ V. L. Rykov,⁴⁸ S. S. Ryu,⁶³ B. Sahlmueller,³⁸ N. Saito,^{31,48,49} T. Sakaguchi,^{6,10,61} S. Sakai,⁵⁹ K. Sakashita,^{48,58} H. Sakata,²⁰ V. Samsonov,⁴⁷ H. D. Sato,^{31,48} S. Sato,^{6,27,59} T. Sato,⁵⁹ S. Sawada,²⁷ K. Sedgwick,⁷ J. Seele,¹¹ R. Seidl,²² A. Yu. Semenov,²⁴ V. Semenov,²¹ R. Seto,⁷ D. Sharma,⁶² T. K. Shea,⁶ I. Shein,²¹ A. Shevel,^{47,54} T.-A. Shibata,^{48,58} K. Shigaki,²⁰ M. Shimomura,⁵⁹ T. Shohjoh,⁵⁹ K. Shoji,^{31,48} P. Shukla,⁴ A. Sickles,^{6,55} C. L. Silva,⁵² D. Silvermyr,⁴⁴ C. Silvestre,¹⁴ K. S. Sim,²⁹ B. K. Singh,³ C. P. Singh,³ V. Singh,³ S. Skutnick,²⁴ M. Slunečka,^{8,25} W. C. Smith,¹ A. Soldatov,²¹ R. A. Soltz,³³ W. E. Sondheim,³⁴ S. P. Sorensen,⁵⁷ I. V. Sourikova,⁶ F. Staley,¹⁴ P. W. Stankus,⁴⁴ E. Stenlund,³⁶ M. Stepanov,⁴³ A. Ster,²⁸ S. P. Stoll,⁶ T. Sugitate,²⁰ C. Suire,⁴⁵ A. Sukhanov,⁶ J. P. Sullivan,³⁴ J. Sziklai,²⁸ T. Tabaru,⁴⁹ S. Takagi,⁵⁹ E. M. Takagui,⁵² A. Taketani,^{48,49} R. Tanabe,⁵⁹ K. H. Tanaka,²⁷ Y. Tanaka,⁴¹ K. Tanida,^{48,49} M. J. Tannenbaum,⁶ A. Taranenko,⁵⁴ P. Tarján,¹⁵ H. Themann,⁵⁵ T. L. Thomas,⁴² M. Togawa,^{31,48} A. Toia,⁵⁵ J. Tojo,⁴⁸ L. Tomášek,²³ Y. Tomita,⁵⁹ H. Torii,^{20,48} R. S. Towell,¹ V.-N. Tram,³² I. Tserruya,⁶² Y. Tsuchimoto,^{20,48} S. K. Tuli,³ H. Tydesjö,³⁶ N. Tyurin,²¹ C. Vale,²⁴ H. Valle,⁶⁰ H. W. van Hecke,³⁴ A. Veicht,²² J. Velkovska,⁶⁰ R. Vertesi,¹⁵ A. A. Vinogradov,³⁰ M. Virius,¹³ V. Vrba,²³ E. Vznuzdaev,⁴⁷ M. Wagner,^{31,48} D. Walker,⁵⁵ X. R. Wang,⁴³ Y. Watanabe,^{48,49} F. Wei,²⁴ J. Wessels,³⁸ S. N. White,⁶ N. Willis,⁴⁵ D. Winter,¹² C. L. Woody,⁶ M. Wysocki,¹¹ W. Xie,^{7,49} Y. L. Yamaguchi,⁶¹ K. Yamaura,²⁰ R. Yang,²² A. Yanovich,²¹

Z. Yasin,⁷ J. Ying,¹⁹ S. Yokkaichi,^{48,49} G. R. Young,⁴⁴ I. Younus,⁴² I. E. Yushmanov,³⁰ W. A. Zajc,¹² O. Zaudtke,³⁸
C. Zhang,^{12,44} S. Zhou,⁹ J. Zimányi,^{28,*} and L. Zolin²⁵

(PHENIX Collaboration)

¹Abilene Christian University, Abilene, Texas 79699, USA

²Institute of Physics, Academia Sinica, Taipei 11529, Taiwan

³Department of Physics, Banaras Hindu University, Varanasi 221005, India

⁴Bhabha Atomic Research Centre, Bombay 400 085, India

⁵Collider-Accelerator Department, Brookhaven National Laboratory, Upton, New York 11973-5000, USA

⁶Physics Department, Brookhaven National Laboratory, Upton, New York 11973-5000, USA

⁷University of California-Riverside, Riverside, California 92521, USA

⁸Charles University, Ovocný trh 5, Praha 1, 116 36, Prague, Czech Republic

⁹China Institute of Atomic Energy (CIAE), Beijing, People's Republic of China

¹⁰Center for Nuclear Study, Graduate School of Science, University of Tokyo, 7-3-1 Hongo, Bunkyo, Tokyo 113-0033, Japan

¹¹University of Colorado, Boulder, Colorado 80309, USA

¹²Columbia University, New York, NY 10027 and Nevis Laboratories, Irvington, New York 10533, USA

¹³Czech Technical University, Zikova 4, 166 36 Prague 6, Czech Republic

¹⁴Dapnia, CEA Saclay, F-91191, Gif-sur-Yvette, France

¹⁵Debrecen University, H-4010 Debrecen, Egyetem tér 1, Hungary

¹⁶ELTE, Eötvös Loránd University, H-1117 Budapest, Pázmány P. s. 1/A, Hungary

¹⁷Florida Institute of Technology, Melbourne, Florida 32901, USA

¹⁸Florida State University, Tallahassee, Florida 32306, USA

¹⁹Georgia State University, Atlanta, Georgia 30303, USA

²⁰Hiroshima University, Kagamiyama, Higashi-Hiroshima 739-8526, Japan

²¹IHEP Protvino, State Research Center of Russian Federation, Institute for High Energy Physics, Protvino, RU-142281, Russia

²²University of Illinois at Urbana-Champaign, Urbana, Illinois 61801, USA

²³Institute of Physics, Academy of Sciences of the Czech Republic, Na Slovance 2, 182 21 Prague 8, Czech Republic

²⁴Iowa State University, Ames, Iowa 50011, USA

²⁵Joint Institute for Nuclear Research, RU-141980 Dubna, Moscow Region, Russia

²⁶KAERI, Cyclotron Application Laboratory, Seoul, Korea

²⁷KEK, High Energy Accelerator Research Organization, Tsukuba, Ibaraki 305-0801, Japan

²⁸KFKI Research Institute for Particle and Nuclear Physics of the Hungarian Academy of Sciences (MTA KFKI RMKI),
H-1525 Budapest 114, P. O. Box 49, Budapest, Hungary

²⁹Korea University, Seoul, 136-701, Korea

³⁰Russian Research Center "Kurchatov Institute," Moscow, Russia

³¹Kyoto University, Kyoto 606-8502, Japan

³²Laboratoire Leprince-Ringuet, Ecole Polytechnique, CNRS-IN2P3, Route de Saclay, F-91128, Palaiseau, France

³³Lawrence Livermore National Laboratory, Livermore, California 94550, USA

³⁴Los Alamos National Laboratory, Los Alamos, New Mexico 87545, USA

³⁵LPC, Université Blaise Pascal, CNRS-IN2P3, Clermont-Fd, 63177 Aubiere Cedex, France

³⁶Department of Physics, Lund University, Box 118, SE-221 00 Lund, Sweden

³⁷Department of Physics, University of Massachusetts, Amherst, Massachusetts 01003-9337, USA

³⁸Institut für Kernphysik, University of Muenster, D-48149 Muenster, Germany

³⁹Muhlenberg College, Allentown, Pennsylvania 18104-5586, USA

⁴⁰Myongji University, Yongin, Kyonggido 449-728, Korea

⁴¹Nagasaki Institute of Applied Science, Nagasaki-shi, Nagasaki 851-0193, Japan

⁴²University of New Mexico, Albuquerque, New Mexico 87131, USA

⁴³New Mexico State University, Las Cruces, New Mexico 88003, USA

⁴⁴Oak Ridge National Laboratory, Oak Ridge, Tennessee 37831, USA

⁴⁵IPN-Orsay, Université Paris Sud, CNRS-IN2P3, BPI, F-91406, Orsay, France

⁴⁶Peking University, Beijing, People's Republic of China

⁴⁷PNPI, Petersburg Nuclear Physics Institute, Gatchina, Leningrad region, RU-188300, Russia

⁴⁸RIKEN Nishina Center for Accelerator-Based Science, Wako, Saitama 351-0198, JAPAN

⁴⁹RIKEN BNL Research Center, Brookhaven National Laboratory, Upton, New York 11973-5000, USA

⁵⁰Physics Department, Rikkyo University, 3-34-1 Nishi-Ikebukuro, Toshima, Tokyo 171-8501, Japan

⁵¹Saint Petersburg State Polytechnic University, St. Petersburg, Russia

⁵²Universidade de São Paulo, Instituto de Física, Caixa Postal 66318, São Paulo CEP05315-970, Brazil

⁵³System Electronics Laboratory, Seoul National University, Seoul, Korea

⁵⁴Chemistry Department, Stony Brook University, Stony Brook, SUNY, New York 11794-3400, USA

⁵⁵*Department of Physics and Astronomy, Stony Brook University, SUNY, Stony Brook, New York 11794, USA*

⁵⁶*SUBATECH (Ecole des Mines de Nantes, CNRS-IN2P3, Université de Nantes) BP 20722-44307, Nantes, France*

⁵⁷*University of Tennessee, Knoxville, Tennessee 37996, USA*

⁵⁸*Department of Physics, Tokyo Institute of Technology, Oh-okayama, Meguro, Tokyo 152-8551, Japan*

⁵⁹*Institute of Physics, University of Tsukuba, Tsukuba, Ibaraki 305, Japan*

⁶⁰*Vanderbilt University, Nashville, Tennessee 37235, USA*

⁶¹*Waseda University, Advanced Research Institute for Science and Engineering, 17 Kikui-cho, Shinjuku-ku, Tokyo 162-0044, Japan*

⁶²*Weizmann Institute, Rehovot 76100, Israel*

⁶³*Yonsei University, IPAP, Seoul 120-749, Korea*

(Received 20 March 2009; published 31 August 2009)

We report the observation at the Relativistic Heavy Ion Collider of suppression of back-to-back correlations in the direct photon+jet channel in Au + Au relative to $p + p$ collisions. Two-particle correlations of direct photon triggers with associated hadrons are obtained by statistical subtraction of the decay photon-hadron (γ - h) background. The initial momentum of the away-side parton is tightly constrained, because the parton-photon pair exactly balance in momentum at leading order in perturbative quantum chromodynamics, making such correlations a powerful probe of the in-medium parton energy loss. The away-side nuclear suppression factor, I_{AA} , in central Au + Au collisions, is $0.32 \pm 0.12^{\text{stat}} \pm 0.09^{\text{sys}}$ for hadrons of $3 < p_T^h < 5$ in coincidence with photons of $5 < p_T^\gamma < 15$ GeV/ c . The suppression is comparable to that observed for high- p_T single hadrons and dihadrons. The direct photon associated yields in $p + p$ collisions scale approximately with the momentum balance, $z_T \equiv p_T^h/p_T^\gamma$, as expected for a measurement of the away-side parton fragmentation function. We compare to Au + Au collisions for which the momentum balance dependence of the nuclear modification should be sensitive to the path-length dependence of parton energy loss.

DOI: [10.1103/PhysRevC.80.024908](https://doi.org/10.1103/PhysRevC.80.024908)

PACS number(s): 25.75.Dw, 13.85.Qk, 13.20.Fc, 13.20.He

I. INTRODUCTION

Experimental results from RHIC have established the formation of hot and dense matter of a fundamentally new nature in relativistic heavy-ion collisions at $\sqrt{s_{NN}} = 200$ GeV [1]. Energy loss in this dense nuclear matter by color-charged, hard ($E \gtrsim 2$ GeV) partons, and the jets into which they fragment, is generally accepted to be the mechanism responsible for the suppression of the high- p_T hadron yields observed in central $A + A$ collisions [2,3]. In the large multiplicity environment of heavy-ion collisions, two-particle correlations are often used to study jet modification and to infer properties of the medium. For example, high- p_T azimuthal dihadron correlations demonstrate that the degree of dijet away-side suppression depends on the p_T of the “trigger” and “associated” hadrons. At moderate p_T ($\gtrsim 3$ GeV/ c), the jet properties measured through two-particle correlations demonstrate novel features such as shape modifications that are thought to be a manifestation of the response of medium to the energy deposited by the attenuated parton [4].

Dihadron measurements of dijet pairs provide an ambiguous measurement of the energy loss of the away-side parton. The trigger hadron is a product of parton fragmentation and therefore it is not possible to determine, event by event, whether the near-side parton has itself lost energy. Given the steeply falling jet spectrum, the sample of hard scatterings is biased toward configurations in which the parton loses little energy. In particular, it is believed that hadron measurements

are subject to a “surface bias” in which the hard scatterings sampled are likely to occur at the periphery of the overlap zone [5,6]. The away-side parton then is more likely to traverse a maximal path-length through the medium. For a sufficiently opaque medium, the attenuation of the parton may be nearly total, in which case the sensitivity to the average path-length is reduced [7]. Back-to-back, high- p_T hadron pairs may originate preferentially from configurations in which the outgoing parton trajectories are tangential to the surface of the overlap zone [8]. However, dihadron pairs may also originate from vertices deep in the collision zone if a parton has a finite probability to “punch-through” or pass through the medium without interaction [9]. Calculations of the relative importance of these two mechanisms depend both on the model of parton energy loss employed and the density profile of the medium [6,10,11].

Direct photon-jet pairs offer two major advantages in studying energy loss as compared to dijets because of the nature of the photon. First, in contrast to partons, photons do not carry color charge and hence do not interact strongly when traversing the medium [12]. The distribution of hard-scattering vertices sampled by direct photon-triggered correlations is thus unbiased by the trigger condition. Suppression of the opposite jet is averaged over all path lengths given by the distribution of hard-scattering vertices. Second, at the Born level, direct photon production in $p + p$ and $A + A$ collisions is dominated by the QCD Compton scattering process, $q + g \rightarrow q + \gamma$, and the photon momentum in the center-of-mass frame is exactly balanced by that of the recoil quark. Higher-order effects and other complications to this idealized picture, such as next-to-leading order (NLO) $2 \rightarrow 3$ bremsstrahlung and other “fragmentation” photons or soft gluon radiation, also do

*Deceased.

[†]PHENIX spokesperson: jacak@skipper.physics.sunysb.edu

need to be considered. Nonetheless, the level of suppression can then be related directly to the energy loss of a parton of known initial momentum. In this way, the average path length of the away-side parton may then be varied in a well-controlled manner by selecting events of various momentum differences between the γ - h pair.

For this reason, the γ +jet channel has long been considered the “golden channel” for studying parton energy loss [13,14]. Neglecting the above-mentioned complications, specifically effects like transverse momentum broadening (the k_T effect) and parton-to-photon fragmentation, back-to-back γ - h correlations in elementary collisions directly measure the fragmentation function of the recoil jet because $z \equiv p^h/p^{\text{jet}} \approx p^h/p^\gamma$. In the standard picture of energy loss, partons are likely to lose some fraction of their energy in the medium but are likely to fragment outside the medium. Hence, the parton energy loss can be considered an effective modification to the fragmentation function. Such a picture may be tested using γ - h correlations in nuclear collisions. Complementary baseline measurements in $p + p$ collisions are used to test the theoretical description of correlations in vacuum and to constrain possible contributions from higher-order processes. Comprehensive reviews of direct photon phenomenology and data from elementary collisions may be found in Refs. [15–17].

II. DETECTOR DESCRIPTION AND PARTICLE IDENTIFICATION

The data were taken with the PHENIX detector [18] using approximately 950 million Au + Au minimum bias events from the 2004 data set and 471 million photon-triggered events from the 2005 and 2006 $p + p$ data sets corresponding to integrated luminosities of 3 (2005) and 10.7 (2006) pb^{-1} . The beam-beam counters (BBC) [19], which are used to trigger the minimum bias data, select 92% of the total inelastic cross section. In Au + Au the BBC and zero-degree calorimeters (ZDC) were used for offline minimum bias event selection and centrality determination. In $p + p$ collisions a high-energy photon trigger, defined by coincidence between the BBC and a high-energy electromagnetic calorimeter (EMCal) tower hit, was used. This EMCal based trigger [20] had an efficiency of $>90\%$ for events with photons and π^0 with energies in the range used in the analysis and within the detector’s geometric acceptance.

The PHENIX central arms, each covering ± 0.35 units of pseudorapidity around midrapidity and 90° in azimuth, contain charged-particle tracking chambers and electromagnetic calorimeters [21]. The EMCal [22] consists of two types of detectors, six sectors of lead-scintillator (PbSc) sampling calorimeters and two of lead-glass (PbG) Cerenkov calorimeters measuring EM energy with intrinsic resolution $\sigma_E/E = 8.1\%/\sqrt{E} \oplus 2.1\%$ and $5.9\%/\sqrt{E} \oplus 0.8\%$, respectively. The fine segmentation of the EMCal ($\Delta\eta \times \Delta\phi \sim 0.01 \times 0.01$ for PbSc and $\sim 0.008 \times 0.008$ for PbG) allows for the reconstruction of π^0 and η mesons in the 2γ decay channel out to p_T of 20 GeV/ c . The details of direct photon and π^0 - and η -meson detection and reconstruction within PHENIX have been described previously [12,23,24]. Photon

candidates with very high purity ($>98\%$ for energies >5 GeV) are selected from EMCal clusters with the use of cluster shower shape and charged particle veto cuts. Two-photon π^0 and η candidates are selected from photon pairs with pair invariant mass in the appropriate π^0 or η mass range. Combinatorial 2γ background is reduced with cuts on energy asymmetry $\alpha_{12} = |E_1 - E_2|/(E_1 + E_2)$, described in detail below. Some fraction of π^0 with p_T starting at ≈ 13 GeV/ c (in the PbSc detector) will appear as a single merged cluster, but with anomalous shower shape, and thus are removed from the analysis. The π^0 and η mesons in the p_T range from about 4 to 17 GeV/ c and photons between 5 and 15 GeV/ c are used in this analysis. For γp_T between 13 and 15 GeV/ c there is a $<2\%$ contribution of merged π^0 cluster contamination; however, this together with all sources of nonphoton contamination are found to have a negligible impact on the two-particle correlation analysis of this report. Direct photons and their two-particle correlations are obtained by statistical subtraction of the estimated meson (mainly π^0) decay photon contribution from the inclusive photon and γ - h samples.

Charged hadrons are detected with the PHENIX tracking system [25] that employs a drift chamber in each arm spanning a radial distance of 2.0–2.4 m from the beam axis with a set of pixel pad chambers (PC1) directly behind them. The momentum resolution was determined to be $\delta p/p = 0.7\% \oplus 1.0\% p$, where p is measured in GeV/ c . Secondary tracks from decays and conversions are suppressed by matching tracks to hits in a second pad chamber (PC3) at distance of ~ 5.0 m. Track projections to the EMCal plane are used to veto photon candidates resulting from charged hadrons that shower in the EMCal.

III. METHOD

A. Two-particle correlations

Two-particle correlations are constructed by measuring the yield of particle pairs as a function of the measured azimuthal angle between photon or parent meson triggers and charged hadron partners. The correlation function, $C(\Delta\phi) \equiv N_{\text{real}}^{\text{pair}}(\Delta\phi)/N_{\text{mixed}}^{\text{pair}}(\Delta\phi)$, corrects for the limited acceptance of γ - h or meson-hadron pairs by dividing the distribution in real events $N_{\text{real}}^{\text{pair}}$ by the mixed event distribution $N_{\text{mixed}}^{\text{pair}}$. The correlation function is decomposed utilizing a two-source model of pair yields coming from two-particle jet correlations superimposed on a combinatorial background yield from an underlying event. The underlying event in Au + Au is known to have an azimuthal asymmetry of harmonic shape quantified in the elliptic flow parameter v_2 [26,27]. This flow represents a harmonic modulation of the $\Delta\phi$ distribution of this underlying event such that the flow-subtracted jet correlation signal is encoded in the jet pair ratio function, $JPR(\Delta\phi) \equiv C(\Delta\phi) - \xi(1 + 2\langle v_2^j \rangle \langle v_2^h \rangle \cos 2\Delta\phi)$, using the notation of Ref. [4], where $\langle v_2 \rangle$ is the average single-particle v_2 .

Two methods of determining the background level ξ , known as zero-yield at minimum (ZYAM) and absolute normalization (ABS), respectively, were applied to the Au + Au data. Both methods are described in detail in previous PHENIX publications [4]; see also Refs. [4,28,29] (ABS) and [30]

(ZYAM). ZYAM assigns the level of zero jet yield and hence ξ to the minimum point of the correlation function $C(\Delta\phi)$. The ABS method uses the mean multiplicity of trigger-associated pairs in mixed events and a correction for finite centrality resolution to determine ξ . Where ZYAM statistical precision is reasonable, the direct γ -h extraction of the two methods agree to within much better than the total uncertainties, typically within $\leq 20\%$. The ABS method is chosen for the Au + Au results presented, as this method resulted in a more precise extraction of direct photon-jet pair yields at high trigger p_T where lack of statistics near $\Delta\phi = \pi/2$ severely impairs the ZYAM determination. In the comparatively low multiplicity $p + p$ collisions, the underlying event originates from different physical mechanisms than in Au + Au and is known not to be well described by event mixing. Instead the correlation functions are normalized by fitting to a double Gaussian + constant function, corresponding to the ZYAM method [4].

The results presented here are corrected for the associated charged hadron efficiency ϵ_h such that the quoted yields correspond to a detector with full azimuthal acceptance and $|\eta| < 0.35$ coverage. No correction is applied for the $\Delta\eta$ acceptance of pairs. Final results are presented in terms of the yield Y of jet pairs per trigger, $Y \equiv A \times JPR(\Delta\phi)/N_{\text{trigger}}$ with the constant $A = \int N_{\text{mixed}}^{\text{pair}}(\Delta\phi)/(2\pi\epsilon_h)$.

The magnitudes of elliptic flow were determined by measuring the distributions of inclusive photons, neutral pions, and charged hadrons as a function of the angle relative to the reaction plane, which was determined with the BBC's as described in Ref. [31]. The v_2 values measured for this analysis are consistent with previous PHENIX analyses [26,27,32].

At high- p_T (≥ 6 GeV/c) the measured $\pi^0 v_2$ values used in the determination of the decay photon v_2 are fit to a constant function to reduce the effects of large statistical fluctuations. The p_T independence of v_2 of π^0 's is motivated by recent preliminary data [33] and by the observed p_T independence of the R_{AA} , because parton energy loss is expected to be the dominant mechanism for azimuthal asymmetry generation at

high- p_T [7]. It is also consistent with the findings of Ref. [32] that is direct measurement of $\pi^0 v_2$ for the same data set and is being published concurrently with this measurement. Because, as discussed in that publication, the high- p_T functional behavior for this data set cannot be well constrained, the level of uncertainty we assign to the constant fit assumption increases with p_T . It is further assumed that the v_2 for other mesons that contribute decay photons (e.g., η) are the same as that of the π^0 at high p_T . For the p_T range considered ($\gtrsim 4.5$ GeV/c) this assumption is also well motivated under the same expectation of v_2 being due to jet quenching, because R_{AA} suppression is already measured to be the same for a variety of mesons (e.g., η itself [24]). Additionally, other high- $p_T v_2$ data measurements confirm the expectation [34] for other hadron species.

Table I lists the v_2 values for the inclusive and π^0 decay photons for all p_T ranges used, either the measurements, or for the highest p_T decay v_2 values from the constant fit value. For the fit values the fit errors are listed as statistical error, despite the inherent systematic correlation of the fit value across the p_T bins. The reduction of the statistical error for decay γv_2 due to fit procedure is clear from comparison to statistical error on the inclusive γv_2 , for which no such fit procedure is used. The assumptions justifying the fit procedure do not apply to the inclusive photons because of their large fraction of direct photons. Direct photon v_2 , if present, is not expected to be influenced by the same energy loss mechanisms. The decay photon v_2 is derived from the measured $\pi^0 v_2$ by the same $p_T^{\pi^0} \rightarrow p_T^{\text{decay } \gamma}$ mapping procedure applied to the yields, described below, though the difference between π^0 and decay v_2 values are negligible compared to the other uncertainties. Listed v_2 systematic uncertainties come only from reaction plane resolution propagated into each p_T bin [4,31]. This procedure has a component that depends again on the statistics in each bin and thus can fluctuate in relative size. The decay γ values are not corrected for π^0 combinatoric background that is discussed below along with the relevant associated systematic error for the estimated for the final jet yield results.

TABLE I. v_2 values used in the jet function extraction for inclusive and decay photons in Au + Au collisions.

Centrality	p_T^{γ}	Inclusive γ			Decay γ		
		v_2	Stat.	Sys.	v_2	Stat.	Sys.
0–20%	5–7	0.053	± 0.009	± 0.011	0.084	± 0.009	± 0.004
	7–9	0.047	± 0.022	± 0.015	0.069	± 0.018	± 0.003
	9–12	0.024	± 0.042	± 0.017	0.069	± 0.020	± 0.003
	12–15	0.064	± 0.096	± 0.094	0.069	± 0.023	± 0.003
20–40%	5–7	0.096	± 0.010	± 0.005	0.155	± 0.011	± 0.036
	7–9	0.079	± 0.027	± 0.011	0.105	± 0.019	± 0.025
	9–12	0.025	± 0.050	± 0.049	0.105	± 0.020	± 0.025
	12–15	0.287	± 0.128	± 0.104	0.105	± 0.023	± 0.024
40–60%	5–7	0.143	± 0.023	± 0.035	0.136	± 0.022	± 0.010
	7–9	0.146	± 0.064	± 0.026	0.126	± 0.039	± 0.008
	9–12	0.162	± 0.126	± 0.252	0.126	± 0.042	± 0.008
	12–15	–0.603	± 0.308	± 0.191	0.126	± 0.046	± 0.008

B. Direct γ -hadron correlation subtraction

A direct photon is defined here to be any photon not from a decay process. Direct photons cannot be identified in Au + Au with reasonable purity on an event-by-event basis due to the large background of meson decay in the p_T range of the analysis and the inability to use isolation cuts in the high multiplicity Au + Au environment. Thus both direct γ and γ - h pairs must be determined from the already-mentioned statistical subtraction procedure, which is therefore consistently used in this report for both the $p + p$ and Au + Au.

Single direct photons have previously been measured in PHENIX for Au + Au [12] and $p + p$ [35]. In these analyses, the estimated yield of decay photons N_{decay}^γ is subtracted from a measured sample of inclusive photons $N_{\text{inclusive}}^\gamma$ resulting in the direct photon yield. These measurements serve as an input to the current analysis, as they fix the fraction of the photon triggers that are expected to be direct. This fraction is quantified by the fraction $R_\gamma \equiv N_{\text{inclusive}}^\gamma / N_{\text{decay}}^\gamma$. The R_γ values used in this analysis are extracted from previous PHENIX measurements, [36,37] by interpolating to obtain the p_T binning used in this analysis. These interpolated values together with the error estimations are tabulated in Table II.

The per-trigger yield of inclusive γ - h pairs $Y_{\text{inclusive}}$ is simply the weighted average of the contributions from decay and direct photon triggers,

$$Y_{\text{inclusive}} = \frac{N_{\text{direct}}^\gamma Y_{\text{direct}} + N_{\text{decay}}^\gamma Y_{\text{decay}}}{N_{\text{inclusive}}^\gamma}. \quad (1)$$

Having already determined R_γ , Y_{direct} may then be obtained by simple manipulation of the above terms. This results in a statistical subtraction that involves only per-trigger yields. Solving for Y_{direct} and rewriting in terms of R_γ we obtain the

TABLE II. Extracted R_γ values used as input to direct γ - h per-trigger yield subtraction [Eq. (2)]. These values are interpolated from previous PHENIX measurements as described in the text.

Centrality	p_T^γ	R_γ	Stat.	Sys.
0–20%	5–7	1.77	± 0.09	± 0.06
	7–9	2.45	± 0.09	± 0.18
	9–12	2.99	± 0.11	± 0.41
	12–15	3.66	± 0.24	± 0.68
20–40%	5–7	1.46	± 0.10	± 0.04
	7–9	1.85	± 0.10	± 0.12
	9–12	2.30	± 0.12	± 0.28
	12–15	2.35	± 0.20	± 0.44
40–60%	5–7	1.30	± 0.09	± 0.05
	7–9	1.52	± 0.07	± 0.13
	9–12	1.85	± 0.10	± 0.30
	12–15	1.94	± 0.24	± 0.36
$p + p$	5–7	1.18	± 0.01	± 0.06
	7–9	1.32	± 0.01	± 0.05
	9–12	1.48	± 0.03	± 0.05
	12–15	1.57	± 0.09	± 0.07

subtraction formula:

$$Y_{\text{direct}} = \frac{R_\gamma Y_{\text{inclusive}} - Y_{\text{decay}}}{R_\gamma - 1}. \quad (2)$$

The direct γ or direct γ - h pair yields do not, by definition, exclude photons from jet fragmentation or medium induced photon production.

C. Extraction of decay photon correlations

The decay photon associated yields are estimated from the measured π^0 - h and η - h correlations through a calculation that determines the decay correlations statistically from a Monte Carlo (MC) based, pair-by-pair weighting procedure. In this procedure the decay γ - h pair yield $N_{\text{decay}}^{\gamma-h}(p_T^\gamma)$ is constructed by a weighted integral over all π^0 - h and η - h pairs. In what follows, we will first describe the procedure schematically, describing the ingredients and how they are obtained. We then give a more exact description and associated formula representing exactly how the weighting was performed in the measurement. Schematically the procedure may be expressed as a convolution of several factors according to the following relation, wherein for simplicity we only consider photons from π^0 decay, although the procedure is also applied to η -decay photons.

$$N_{\text{decay}}^{\gamma-h}(p_T^\gamma) = \int \frac{\epsilon_\gamma(p_T^\gamma, p_T^\pi) \otimes \mathcal{P}(p_T^\gamma, p_T^\pi)}{\epsilon_\pi(p_T^\pi)} \otimes N^{\pi-h}(p_T^\pi), \quad (3)$$

where ϵ_π and ϵ_γ are the π^0 and single *decay* photon efficiencies, respectively, and \mathcal{P} is the decay probability density, each of which is addressed in turn below.

First, because the starting point is the uncorrected raw meson- h pair yield $N^{\pi-h}$, a correction for the parent meson reconstruction efficiency, $\epsilon_\pi(p_T^\pi)$, is applied to the raw π^0 's as a function of p_T to account for the π^0 daughter photons in the inclusive sample whose sisters lie outside the PHENIX acceptance or are otherwise undetected. Both efficiencies, ϵ_γ and ϵ_π , in Eq. (3) are also evaluated as a function of the position in the calorimeter along the beam direction; however, this dependence mostly cancels in the ratio $\epsilon_\gamma/\epsilon_\pi$ and therefore is suppressed for clarity. The value of $\epsilon_\pi(p_T^\pi)$ is determined by dividing the raw number of π^0 's $N^\pi(p_T^\pi)$ obtained in the same data sample by our published π^0 invariant yields [2,24,38] assuming no pseudorapidity dependence over the narrow PHENIX acceptance. The top panel in Fig. 1 illustrates, for the example of central Au + Au events, the π^0 efficiency correction factor $1/\epsilon_\pi(p_T^\pi)$. The correction rises at small p_T due to a p_T -dependent pair energy asymmetry cut designed to reduce combinatorial 2γ pairs reconstructed as real π^0 's. This cut, along with the effects of any remaining background, is described below. At large p_T the quantity $1/\epsilon_\pi(p_T^\pi)$ rises again due to losses from cluster merging.

Second, the effect of decay kinematics is evaluated by determining the probability density, $\mathcal{P}(p_T^\gamma, p_T^\pi)$, for the decay of a p_T -independent distribution of π^0 's. $\mathcal{P}(p_T^\gamma, p_T^\pi)$ represents the relative probability of a π^0 of $p_T = p_T^\pi$, to decay into a photon of p_T^γ . For a perfect detector, this function is calculable analytically. A simple fast MC generator implements the

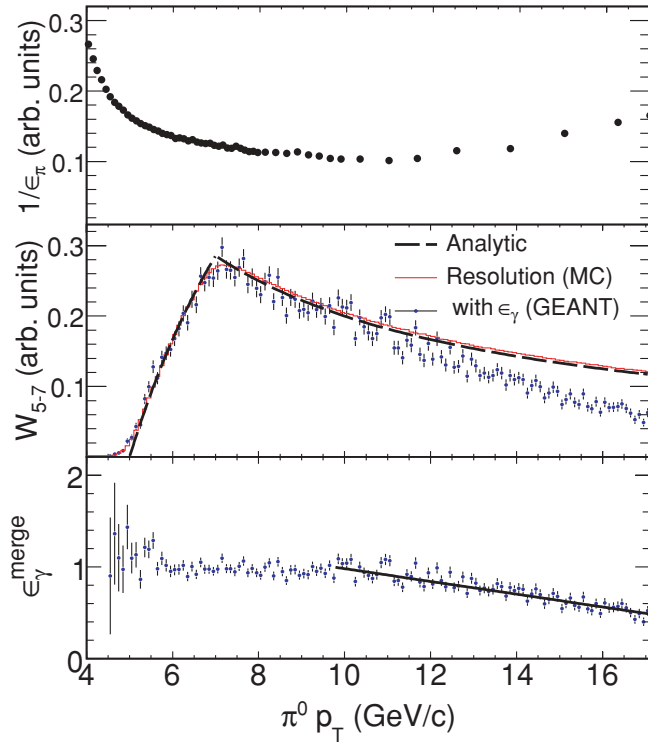


FIG. 1. (Color online) The weight factors used to obtain decay correlations from parent meson correlations. (Top) π^0 reconstruction efficiency correction, $1/\epsilon_\pi$, shown in arbitrary units. (Middle) Decay probability function, W_{ab} , also in arbitrary units, for 5–7 GeV/c decay photons from π^0 derived analytically (black line), using the detector acceptance and resolution smearing (red line) and including the single decay photon efficiency, ϵ_γ , from a GEANT simulation (blue points). (Bottom) $\epsilon_\gamma^{\text{merge}}$ obtained by taking ratio of the blue points to red curve in the previous panel.

PHENIX acceptance and uses Gaussian smearing functions to simulate detector resolution according to the known EMCAL energy and position resolution. Occupancy effects give rise to an additional smearing of the π^0 and η invariant masses. This effect is included in the MC by tuning the resolution parameters to match the π^0 peak widths observed in data. False reconstruction of π^0 's and η 's from combinatorial matches are either subtracted or assigned to the systematic uncertainties as discussed below.

Finally, we wish to estimate the decay photon contribution to the measured raw inclusive photon sample that differs from the true decay photon distribution by the single decay photon efficiency, $\epsilon_\gamma(p_T^\pi)$. At intermediate p_T , $\epsilon_\gamma(p_T^\pi)$ depends only on the photon momentum and is included already implicitly by the fast MC simulation described above to produce $\mathcal{P}(p_T^\gamma, p_T^\pi)$. Thus, it is useful to think of them as a single factor $W(p_T^\gamma, p_T^\pi) \equiv \mathcal{P}(p_T^\gamma, p_T^\pi)\epsilon_\gamma(p_T^\gamma, p_T^\pi)$. At high p_T , however, an efficiency loss is incurred by photons from π^0 's whose showers merge into a single cluster in the calorimeter and are rejected by the shower-shape cut. As a consequence, the fraction of photons that are direct is artificially enhanced in the sample of reconstructed photon clusters. The single decay photon efficiency depends on both the parent and daughter p_T and is evaluated in a GEANT simulation. In principle the

convolution of both $\mathcal{P}(p_T^\gamma, p_T^\pi)$ and $\epsilon_\gamma(p_T^\gamma, p_T^\pi)$, $W(p_T^\gamma, p_T^\pi)$ could be extracted as one function from the GEANT simulation, but obtaining large-enough MC statistics necessary to properly parametrize the above-mentioned EMCAL z position dependence of the $\epsilon_{\pi,\gamma}$ corrections is feasible only with the fast MC. Thus only the efficiency loss by cluster merging for photons $\epsilon_\gamma^{\text{merge}}$ is taken from the GEANT. The bottom panel of Fig. 1 shows $\epsilon_\gamma^{\text{merge}}(p_T^\pi)$ evaluated from the GEANT simulation.

Because we wish to construct per-trigger yields, the same procedure described in Eq. (3) can be applied to find the estimated single decay photon trigger yield from the measured single π^0 's, i.e., replacing $N_{\text{decay}}^{\gamma-h}$ with N_{decay}^γ and $N^{\pi-h}$ with N^π . The exact application of schematic Eq. (3) then takes the form of a sum over all π^0 -h pairs and single π^0 's found in the data. Each π^0 or π^0 -h pair is given a weight that depends on $\pi^0 p_T$. Operationally we now split this weight into two parts: $\epsilon_\pi(p_T^\pi)$ discussed above and a factor $W_{ab}(p_T^\pi)$. The factor W_{ab} is simply the end result of the fast MC-GEANT combined calculation, the convolution of \mathcal{P} and ϵ_γ , including $\epsilon_\gamma^{\text{merge}}$, averaged over a chosen decay photon bin of the range $a < p_T < b$. Thus in terms of the product $W(p_T^\gamma, p_T^\pi)$ then $W_{ab}(p_T^\pi)$ is given by

$$W_{ab}(p_T^\pi) = \int_a^b dp_T^\gamma W(p_T^\pi, p_T^\gamma). \quad (4)$$

The functions $W_{ab}(p_T^\pi)$ are defined for the four photon p_T bins used in the analysis, $[a, b] = [5, 7]$, $[7, 9]$, $[9, 12]$, and $[12, 15]$ GeV/c. An example of $W_{ab}(p_T^\pi)$ for the 5- to 7-GeV/c bin is shown in Fig. 1. Procedurally, we construct W_{ab} as product of the fast MC curve shown in the middle panel and the linear fit discussed above to the bottom panel, $\epsilon_\gamma^{\text{merge}}(p_T^\pi)$. Although a decay of $p_T^\pi < a$, the lower limit of the decay p_T bin, is kinematically disallowed, W_{ab} is nonzero below this boundary when resolution effects are considered. For $p_T^\pi > b$, W_{ab} decreases as $\sim 1/p_T^\pi$, slowly enough that π^0 's at values of p_T beyond the statistical reach of the data set contribute to the relevant decay photon p_T selections at a non-negligible rate. The π^0 sample is truncated at $p_T = 17$ GeV/c and extrapolated using power-law fits to the single and conditional π^0 spectra to estimate a correction. In the latter case, each associated hadron p_T range is fit independently. The truncation avoids the high- p_T region where cluster merging effects are dominant and the $1/\epsilon^\pi$ correction factor becomes large. Although the truncation corrections for the number of decay photons and decay γ -h pairs are non-negligible, they mostly cancel in the per-trigger yield and are therefore typically $< 1\%$, reaching a maximum value of 7% for only the $12 < p_T^\gamma < 15 \otimes 3 < p_T^\pi < 5$ GeV/c bin.

With the weight functions W_{ab} the entire set of π^0 -hadron pairs and single π^0 candidates (within a given range of $\Delta\phi$, $\phi_1 < \Delta\phi < \phi_2$, defining each $\Delta\phi$ bin) are then summed over, once for each decay photon p_T bin, and the per-trigger yield is constructed for each of these decay p_T bins as

$$Y_{\text{decay}} \Big|_{a < p_T^\gamma < b}^{\phi_1 < \Delta\phi_{\pi-h} < \phi_2} = \frac{\sum_{i=1-N^{\pi-h}}^{\phi_1 < \Delta\phi_{\pi-h} < \phi_2} W_{ab}(p_{Ti}^\pi) / \epsilon_\pi(p_{Ti}^\pi)}{\sum_{i=1-N^\pi} W_{ab}(p_{Ti}^\pi) / \epsilon_\pi(p_{Ti}^\pi)}. \quad (5)$$

In this form it is clear that the normalization of the functions $\epsilon_\pi(p_T^\pi)$ and $W_{ab}(p_T^\pi)$ cancel out completely in the per-trigger yield, and therefore only their shapes versus p_T^π are important. Hence in Fig. 1 the curves are shown with arbitrary units. Also, as Eq. (5) implies, the angular deviation between the direction of a decay photon and its parent meson is ignored. The $\Delta\phi$ opening angle of a decay photon and hadron pair is taken to be the same as the $\Delta\phi_{\pi-h}$ of the parent π^0 -h pairs. This approximation is tested in the fast MC and found to be extremely accurate because the distribution of angular deviation between a leading decay photon in a 2γ decay and the parent mesons at these π^0 momenta have an rms around 0 of $\ll 0.01$ radians, and the smallest $\Delta\phi$ bins considered in the analysis are typically ~ 0.1 radians or larger.

D. π^0 and η reconstruction

In $p + p$ collisions Y_{decay} is estimated using both reconstructed π^0 and η mesons in invariant mass windows of 120–160 and 530–580 MeV/c², respectively. The total decay per-trigger yield is calculated from

$$Y_{\text{decay}} = (1 - \delta_{h/\pi^0}^Y) Y_{\text{decay}}^{\pi^0} + \delta_{h/\pi^0}^Y Y_{\text{decay}}^\eta, \quad (6)$$

where δ_{h/π^0}^Y is the ratio of the total number of decay photons to the number of decay photons from π^0 . Based on the measurements of η [24] and ω [39], which together with the π^0 account for $>99\%$ of decay photons, the value of δ_{h/π^0}^Y is determined to be 1.24 ± 0.05 in the high- p_T region covered by this analysis, independent of collision system and centrality. Note that the per-trigger yields for ω and other heavier meson triggers ($\omega, \eta', \phi, \dots$) are not measured and are taken to be equivalent to Y_{decay}^η in Eq. (6). This assumption was studied in PYTHIA and found to influence Y_{decay} at the level of $<2\%$. In Au + Au collisions correlations using η triggers are not directly measured but rather estimated from the $p + p$ measurement as discussed below.

Figure 2 shows the various components of the decay photon measurement in $p + p$. In $p + p$ collisions the rate of combinatorial background photon pairs is reduced by considering only photons of $p_T > 1$ GeV/c resulting in background levels of $<10\%$ for which no correction was applied. The effect of such remaining pairs on $Y_{\text{decay}}^{\pi^0}$ was evaluated to be negligible ($<2\%$) compared to the size of other uncertainties on the final Y_{direct} result using a detailed full PYTHIA test of the method that included π^0 reconstruction with combinatorial photon pairs. However, η reconstruction has a much smaller signal-to-background of 1.4–1.6, depending on the p_T selection, even in the low multiplicity $p + p$ environment. In this case, the per-trigger yield of the combinatorial photon pairs is estimated from photon pairs with invariant mass in “sideband” ranges of 400–460 and 640–700 MeV/c², beyond 3σ of the η peak. The sideband contribution $Y_{\text{decay}}^{\text{sideband}}$ is then subtracted using the signal-to-background ratio f_{bkg} evaluated from Gaussian + polynomial background fits to the invariant mass distributions according to $Y_{\text{decay}}^{\text{signal}} = Y_{\text{decay}}^{\text{raw}} / (1/f_{\text{bkg}} + 1) - Y_{\text{decay}}^{\text{sideband}} / f_{\text{bkg}}$. The yield $Y_{\text{decay}}^{\text{sideband}}$ is generated from the full meson to decay photon weighting function procedure [Eq. (5)]. The subtraction procedure was also tested

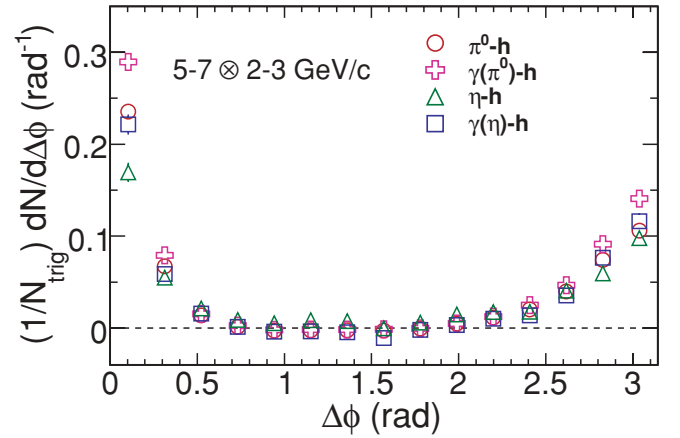


FIG. 2. (Color online) Examples of parent and daughter per-trigger yields for the π^0 and η in $p + p$ collisions for p_T selection $5 < p_T^Y < 7$ and $2 < p_T^h < 3$ GeV/c. These ZYAM correlation measurements, fully corrected for acceptance and efficiency (except the PHENIX rapidity acceptance), are used to determine the total decay photon per-trigger yield as described in the text.

in PYTHIA and the extracted and input per-trigger yields were found to agree to within 10%.

In Au + Au collisions the combinatorial rate for π^0 reconstruction is substantially larger. Correspondingly, a p_T -dependent cut on the pair energy asymmetry $\alpha_{12} = |E_1 - E_2| / (E_1 + E_2)$ [23], visible in Fig. 1 with the smallest allowed asymmetry at the lowest $\pi^0 p_T$ values, is used to reduce this background. With such cuts the signal-to-background in central events varies from 5:1 at its lowest, increasing to about 15:1 for the highest p_T selection. The effect of the combinatorial background is studied through examination of a similar sideband subtraction analysis as in the $p + p \eta - h$ correlation extraction described, this time for π^0 -h, using invariant mass ranges just outside the π^0 peak region. However, no clear trend beyond non-negligible statistical limitations is observed, so no correction for the background is applied. Instead the maximum size of the effect (typically $\simeq 7\%$) is included as source of systematic uncertainty on the decay yields and propagated to the final direct photon per-trigger yields.

In central Au + Au collisions the η meson cannot be reconstructed with sufficient purity to measure its correlations. Instead, a scaling argument is employed. Motivated by the similar high- p_T suppression pattern shown by η and π^0 in Au + Au [24] and corresponding near equality of the $p + p$ and Au + Au η/π^0 ratios, the ratio $Y_{\gamma(\eta)}/Y_{\gamma(\pi^0)}$ is measured in $p + p$ and applied as a correction to the Au + Au $Y_{\gamma(\pi^0)}$. This is justified by the assumption that the jet fragmentation is primarily occurring outside the medium. We do not attribute any additional uncertainty to this scaling beyond the 10% sideband systematic and statistical uncertainties of the η measurement in $p + p$. However, to give an idea of the possible impact of this assumption, the size of the total systematic uncertainty on Y_{decay} from all other sources would be equivalent to a variation of the Au + Au $Y_{\gamma(\eta)}$ by $\sim 50\%$. Given the similarity of the high- p_T suppression demonstrated

by all light quark bound states measured thus far, this would correspond to a rather large change.

IV. SYSTEMATIC UNCERTAINTIES

There are four main classes of systematic uncertainty in the Au + Au data: elliptic flow, normalization of the underlying event (ABS), R_γ , and the decay per-trigger yield estimate, only the latter two of which are present or non-negligible in the $p + p$ data. Table III lists the fractional contribution of each of these sources to the total systematic uncertainty on the direct photon per-trigger yields in the 20% most central Au + Au and $p + p$ data. In the central Au + Au data the uncertainty at low p_T^h is dominated by the v_2 and correlation function normalization (ABS method) estimation due to large multiplicity of hadrons. At higher p_T^h , but low trigger p_T , p_T^t , the decay error dominates due to the two-photon combinatorial background for π^0 reconstruction. Finally, at large p_T^h and p_T^t the backgrounds responsible for both of these sources of uncertainty decrease and the uncertainty on R_γ , which is relatively constant, dominates. In $p + p$ collisions the decay photon background forms a much larger fraction of the total photon sample. In this case, the decay uncertainty arises from the MC decay photon mapping procedure, the η sideband subtraction and the η/π^0 ratio in approximately equal parts. The yields associated with daughter photons are larger than for the meson parents because of feed-down from larger values of parent p_T , and hence, jet p_T .

The correction for single hadron efficiency $\epsilon_h(p_T^h)$ varies as a function of collision system and centrality. These corrections are obtained by finding the ratio of raw yields of hadrons obtained without the trigger condition in the same analysis (i.e., with the same cuts as in the analysis to the previous PHENIX published measurements of the corresponding charged hadron

TABLE III. Fractional contribution to the total systematic uncertainty for each of the main sources of uncertainty in $p + p$ and 0–20% Au + Au collisions. Derived by propagating each uncertainty individually and finding fraction of the total (nonquadrature) sum. For the total systematic uncertainties (see Table IV), sources are added in quadrature as usual.

p_T^y (GeV)	p_T^h (GeV)	Au + Au, centrality 0–20%				$p + p$	
		R_γ	Decay	v_2	Norm.	R_γ	Decay
5–7	1–2	0.03	0.14	0.50	0.33	0.14	0.86
	2–3	0.02	0.32	0.46	0.20	0.21	0.79
	3–5	0.02	0.71	0.18	0.10	0.05	0.95
7–9	1–2	0.09	0.17	0.45	0.29	0.22	0.78
	2–3	0.10	0.35	0.38	0.17	0.25	0.75
	3–5	0.09	0.61	0.18	0.13	0.21	0.79
9–12	1–2	0.06	0.09	0.53	0.33	0.19	0.81
	2–3	0.26	0.25	0.33	0.16	0.30	0.70
	3–5	0.46	0.30	0.13	0.10	0.35	0.65
12–15	1–2	0.08	0.01	0.63	0.29	0.21	0.79
	2–3	0.21	0.14	0.48	0.17	0.02	0.98
	3–5	0.22	0.14	0.39	0.25	0.10	0.90

spectra) [40,41]. As in previous PHENIX two-particle correlation measurements [4,30], this procedure has inherent uncertainties assigned as a p_T -independent 10% uncertainty, on each system and/or centrality.

V. RESULTS

A. Direct γ -h per-trigger yields

Figure 3 shows examples of direct photon per-trigger yields in $p + p$ and central Au + Au collisions. Also shown are the per-trigger yields for inclusive and decay photon triggers that are the ingredients in the statistical subtraction method as expressed in Eq. (2). A clear away-side correlation is observed ($\Delta\phi \simeq \pi$) for direct photons triggers in $p + p$. In Au + Au collisions the away-side correlation is suppressed for both decay and direct photon triggers. The near-side direct photon associated yields are small relative to that of decay photons, an expected signature of prompt photon production [16].

The away-side yields, integrated over $|\Delta\phi - \pi| < \pi/5$ radians, are shown in Fig. 4 and Table IV for $p + p$ and Au + Au collisions. This range roughly corresponds to the “head region” as defined in Ref. [4] and is chosen primarily to minimize the influence of medium response that is thought to dominate the “shoulder” region further offset from $\Delta\phi = \pi$. Additionally, the acceptance and the signal itself are largest in this range so statistical precision is maximized. It should be noted that the width of the jet correlation is larger than this interval. We do not make a correction for this effect, because we are primarily concerned with the comparison of the yields from $p + p$ and Au + Au collisions. It should be noted, however, that in addition to parton energy loss, any broadening of azimuthal correlations, whether by hot or cold nuclear matter effects, will contribute to a suppression in the yield in the head region. Due to statistical and systematic fluctuations, the subtraction of the decay-photon hadron pairs

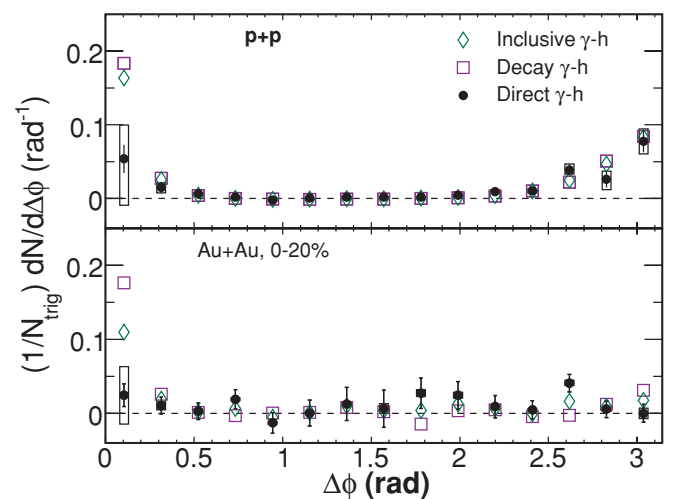


FIG. 3. (Color online) Examples of ZYAM subtracted per-trigger yields, fully corrected for acceptance and efficiency (except rapidity acceptance) used in the direct photon correlation analysis for the $5 < p_T^y < 7$ and $3 < p_T^h < 5$ GeV/c bin. (Top/bottom) Inclusive, decay and direct photon per-trigger yields in $p + p$ (0–20% central Au + Au) collisions.

TABLE IV. Direct γ - h per-trigger yields in 20% most central Au + Au and in $p + p$ collisions. An additional p_T -independent uncertainty of 10% due to the charged hadron efficiency corrections is not shown.

p_T^γ (GeV)	p_T^h (GeV)	$\langle z_T \rangle$	Yield	Stat.	Sys.	Total
Au + Au, centrality 0–20%						
5–7	1–2	0.23	6.26×10^{-2}	4.72×10^{-2}	4.62×10^{-2}	6.60×10^{-2}
	2–3	0.41	2.68×10^{-2}	1.29×10^{-2}	5.68×10^{-3}	1.41×10^{-2}
	3–5	0.62	4.82×10^{-3}	2.13×10^{-3}	1.96×10^{-3}	2.90×10^{-3}
7–9	1–2	0.17	3.71×10^{-2}	8.48×10^{-2}	5.59×10^{-2}	1.02×10^{-1}
	2–3	0.3	3.45×10^{-2}	2.39×10^{-2}	8.46×10^{-3}	2.53×10^{-2}
	3–5	0.46	9.63×10^{-3}	4.18×10^{-3}	1.96×10^{-3}	4.62×10^{-3}
9–12	1–2	0.13	1.28×10^{-1}	1.34×10^{-1}	6.84×10^{-2}	1.51×10^{-1}
	2–3	0.23	3.94×10^{-2}	3.81×10^{-2}	1.01×10^{-2}	3.94×10^{-2}
	3–5	0.36	-2.16×10^{-3}	6.29×10^{-3}	2.06×10^{-3}	6.62×10^{-3}
12–15	1–2	0.1	5.31×10^{-1}	2.53×10^{-1}	1.49×10^{-1}	2.94×10^{-1}
	2–3	0.18	-6.13×10^{-3}	6.99×10^{-2}	1.80×10^{-2}	7.22×10^{-2}
	3–5	0.28	3.25×10^{-2}	1.60×10^{-2}	2.52×10^{-3}	1.62×10^{-2}
$p + p$						
5–7	1–2	0.24	1.44×10^{-1}	9.93×10^{-3}	3.42×10^{-2}	3.56×10^{-2}
	2–3	0.43	4.22×10^{-2}	5.47×10^{-3}	1.20×10^{-2}	1.32×10^{-2}
	3–5	0.66	1.55×10^{-2}	2.07×10^{-3}	3.26×10^{-3}	3.86×10^{-3}
7–9	1–2	0.18	1.73×10^{-1}	1.84×10^{-2}	2.88×10^{-2}	3.42×10^{-2}
	2–3	0.31	6.24×10^{-2}	1.11×10^{-2}	1.15×10^{-2}	1.60×10^{-2}
	3–5	0.48	2.26×10^{-2}	4.53×10^{-3}	3.75×10^{-3}	5.88×10^{-3}
9–12	1–2	0.14	2.59×10^{-1}	2.99×10^{-2}	2.50×10^{-2}	3.90×10^{-2}
	2–3	0.24	7.01×10^{-2}	1.73×10^{-2}	1.00×10^{-2}	2.00×10^{-2}
	3–5	0.38	1.94×10^{-2}	7.21×10^{-3}	3.77×10^{-3}	8.14×10^{-3}
12–15	1–2	0.11	1.20×10^{-1}	5.13×10^{-2}	7.22×10^{-2}	8.86×10^{-2}
	2–3	0.19	1.04×10^{-1}	3.11×10^{-2}	2.02×10^{-2}	3.71×10^{-2}
	3–5	0.3	4.26×10^{-2}	1.62×10^{-2}	1.13×10^{-2}	1.97×10^{-2}

from the inclusive γ - h sample can result in a negative yield. In this case 90% confidence-level upper limits are given. In the case that a positive yield is obtained, but the uncertainty is consistent with 0, the lower bound of the error bar is also replaced with an arrow. As noted in the figure caption, a 10% p_T -independent uncertainty due to the charged hadron efficiency corrections is not shown.

B. Suppression factor I_{AA}

Departure from the vacuum QCD processes is quantified by I_{AA} , the ratio of Au + Au to $p + p$ per-trigger yields:

$$I_{AA}(p_T^\gamma, p_T^h) = \frac{Y^{\text{Au+Au}}(p_T^\gamma, p_T^h)}{Y^{p+p}(p_T^\gamma, p_T^h)}. \quad (7)$$

Figure 5 shows the I_{AA} values for all direct photon and associated hadron bins for the most central 0–20% of collisions. The data points for which the subtraction resulted in a negative yield value (the 90% confidence level upper limits) are included with standard $1\text{-}\sigma$ uncertainties. For the p_T^γ range 5–12 GeV/ c , a significant suppression is observed in the $3 < p_T^h < 5$ GeV/ c bin in which the highest precision

is obtained. At lower p_T^h , where the background subtraction is largest, the data do not have the statistical precision to determine the degree to which the yields are suppressed. I_{AA} for direct photon triggers is consistent to that of charged hadron triggers [4] as shown in the top left panel in which results with similar ranges of $p_{T,i}$ are compared.

Figure 6 shows the I_{AA} for the $p_T^h = 3\text{--}5$ GeV/ c bin, integrated for all trigger p_T bins ($p_T^\gamma = 5\text{--}15$ GeV/ c) and for three centrality bins, 0–20%, 20–40%, and 40–60%. For the most central bin, the suppression of the away-side direct photon per-trigger yield is clearly observed, $I_{AA} = 0.32 \pm 0.12^{\text{stat}} \pm 0.09^{\text{syst}}$. Within large uncertainties we see that the γ -jet I_{AA} in this p_T range, dominated by moderate to high values of z ($\equiv p^h/p^{\text{jet}}$), is consistent with the single-particle R_{AA} as a function of centrality, consistent with a scenario in which the geometry of suppression plays an important role as would be expected from a sample dominated by surface emission.

Figure 6 also compares I_{AA} from a measurement of high- p_T dihadron ($h^\pm - h^\pm$) correlations [4] to the γ -jet result for similar $p_{T,i}$ selections. The two results are remarkably similar in the most central bin. This may indicate that surface emission is dominant for both samples in this z region. However it should

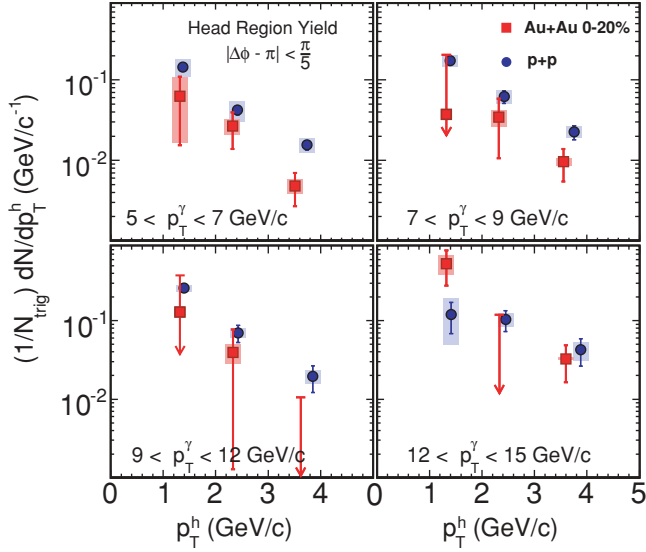


FIG. 4. (Color online) Direct γ - h per-trigger yields for the range $|\Delta\phi - \pi| < \pi/5$ radians vs. associated hadron p_T . Four different direct γp_T ranges (indicated on the figure) are shown in the most central 20% of Au + Au events and $p + p$ events. The upper limits are for 90% confidence levels. A p_T -independent uncertainty of 10% due to the charged hadron efficiency correction is suppressed from the plot.

be noted that the total uncertainties on either measurement are still quite large on a relative scale. Also, because our method does not remove the so-called “fragmentation prompt photon” or NLO direct photon contribution associated with dijet production, a small residual dijet contribution may be present; however, this contribution will be suppressed by R_{AA} relative to that of γ -jet and thus will not affect interpretations

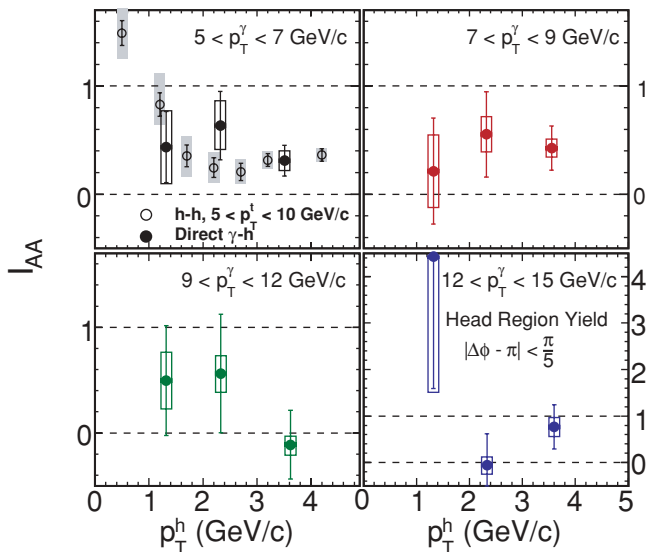


FIG. 5. (Color online) Ratio I_{AA} of the Au + Au to $p + p$ yields shown in Fig. 4. For comparison the first panel shows dihadron correlation data from Ref. [4]. An additional p_T -independent uncertainty of 14% due to the charged hadron efficiency corrections is not shown.

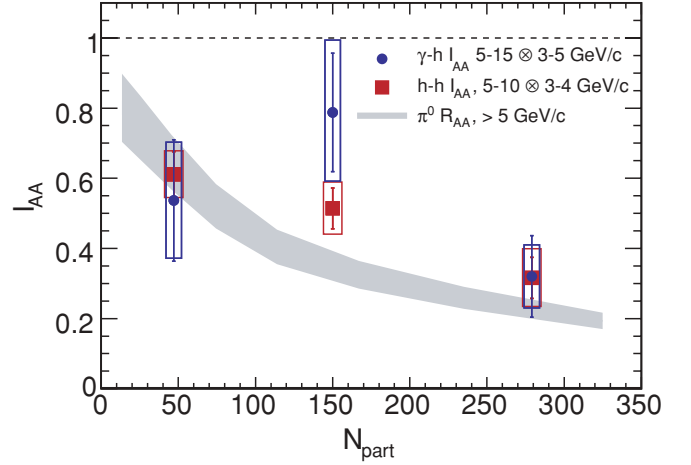


FIG. 6. (Color online) $I_{AA}(p_T^\gamma)$ integrated over the range $5 < p_T^\gamma < 15$ GeV/c for associated hadrons of $3 < p_T^h < 5$ GeV/c vs. centrality compared to single π^0 high- p_T R_{AA} (integrated over $p_T > 5$ GeV/c) [2]. An additional p_T -independent uncertainty of 14% due to the charged hadron efficiency corrections is not shown.

of the data presented here. As explained in the introduction, the dijet and γ -jet measurements should be subject to different geometrical effects. Disentangling such effects through precise comparisons of dihadron and γ - h suppression should be pursued with future measurements with improved statistics.

C. Towards the fragmentation function

Using the distribution of charged hadrons opposite direct γ triggers, parton energy loss may be studied directly as a departure from the (vacuum) fragmentation function. In distinction to π^0 - h correlations, where the away-side distribution is sensitive only to the integral of the fragmentation function (the average multiplicity of the away-side jet) [42], the away-side distribution for direct γ - h correlations provides a measurement of the full fragmentation function of the jet from the away-side parton. To the extent that the transverse momentum of the away-side parton and the direct γ are equal and opposite, as in leading order pQCD, the fragmentation function of the jet from the away-parton should be given to a good approximation by the x_E distribution,

$$x_E = \frac{-\vec{p}_T^t \cdot \vec{p}_T^h}{|\vec{p}_T^t|^2} = \frac{-p_T^h \cos \Delta\phi}{p_T^t}, \quad (8)$$

where the transverse momentum of the trigger $p_T^t = p_T^\gamma$ in the case of γ - h correlations. The reasons why the scaling variable x_E is an approximation to, rather than an exact measure of, the fragmentation variable of the away-side jet with momentum z_a are (i) the away-side parton does not generally balance longitudinal momentum with the trigger γ , although it is restricted by the $\Delta\eta$ acceptance of the detector; (ii) the transverse momenta of the γ and away parton do not exactly balance. The transverse momentum imbalance was discovered at the CERN-ISR using x_E distributions

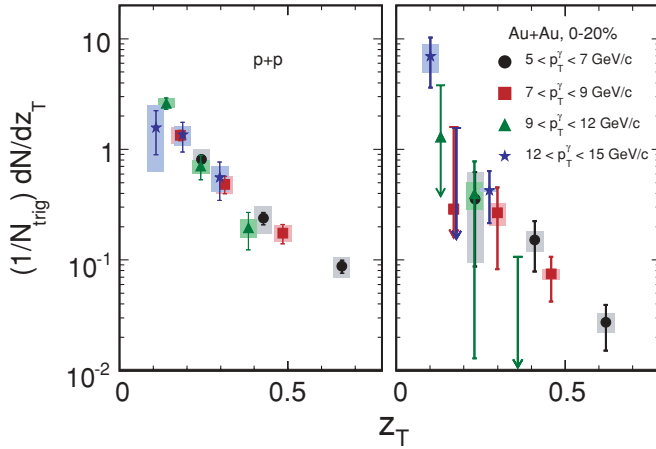


FIG. 7. (Color online) z_T distributions dN/dz_T from the direct photon associated yields in $p + p$ (left) and 0–20% Au + Au (right) collisions.

[43] and originally attributed to an “intrinsic” transverse momentum k_T of each of the initial colliding partons [44], but now understood to be due to “resummation” of soft-gluon effects [45,46].

The validity of the approximation $x_E \approx z_a$ can be tested by observing identical x_E distributions for different values of trigger p_T^γ (x_E scaling), in which case one would accept the x_E distribution in γ -h correlations as the quark fragmentation function from the reaction $q + g \rightarrow q + \gamma$ without need of correction. We approximate x_E by z_T , the ratio of the mean associated p_T^h to mean trigger p_T for each p_T^γ bin.¹ The $\langle p_T^h \rangle$ for the four trigger bins are 5.66, 7.75, 10.07, 13.07 GeV/c, close to the values obtained from a fit to the direct- γ invariant cross section of the form $p_T^{-6.5}$ [35].

Figure 7 shows the z_T distributions for $p + p$ and Au + Au collisions. The $p + p$ data [Fig. 7(a)] exhibit reasonable z_T scaling so that the measured distribution should represent the away-side jet fragmentation function. A fit of this data to a simple exponential (Ne^{-bz_T}) gives an acceptable $\chi^2/\text{DOF} = 12.8/10$ with a value $b = 6.9 \pm 0.8$ that is consistent with the quark fragmentation function, parameterized [42] as a simple exponential with $b = 8.2$ for $0.2 < z < 1.0$, and inconsistent with the gluon fragmentation function value of $b = 11.4$. It should, however, be recalled that the data do not cover the full extent of the away peak, only $|\Delta\phi - \pi| < \pi/5$ radians and that possible variations of the widths of the peaks in both the $p + p$ data and the Au + Au data with p_T^γ and p_T^h have not been taken into account in the present analysis. Additionally a more detailed analysis, differential in trigger p_T , is necessary to study trigger p_T -dependent effects that can influence the fragmentation function fit values [42].

¹The reader is advised to carefully distinguish this variable $z_T = \langle p_T^h \rangle / \langle p_T^\gamma \rangle$ from our previous notation used in Ref. [42] of $z_i = p_T^i / \hat{p}$, which is the fraction of jet momentum \hat{p} contained in the trigger particle.

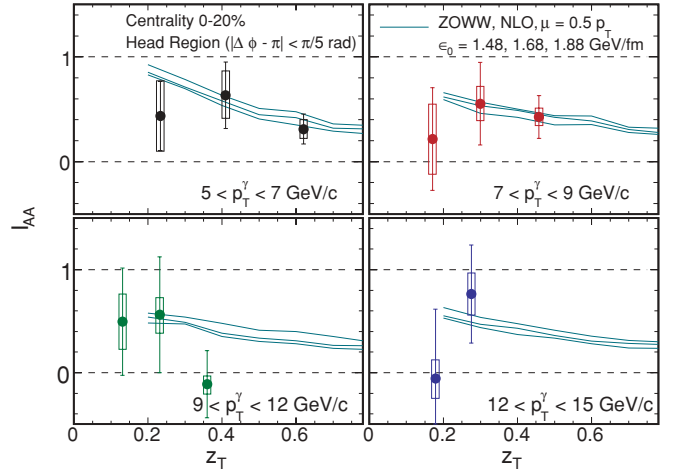


FIG. 8. (Color online) $I_{AA}(z_T)$ for the 20% most central Au + Au data compared to predictions from an energy loss calculation [50]. An additional p_T -independent uncertainty of 14% due to the charged hadron efficiency corrections is not shown.

In central Au + Au collisions, the fragmentation function may be modified by the medium² so z_T scaling should not hold except in two special cases: (i) pure surface emission or punch-through where the away-side jets are not modified (the z_T distribution will be suppressed, but will have the same shape as in $p + p$ collisions); (ii) constant fractional energy loss of the away jet (the z_T scaling will be preserved in Au + Au collisions but with a steeper slope than in $p + p$ collisions). The Au + Au data [Fig. 7(b)] are consistent with z_T scaling with the same shape as the $p + p$ data, a value of $b = 5.6 \pm 2.2$ and excellent $\chi^2/\text{DOF} = 10.1/10$ for the simple exponential fit. The point at lowest $z_T = 0.11$ for Au + Au is 1.6 standard deviations above the fit, suggesting that improved statistics will permit the observation of any nonsurface emission.

D. Model comparison

Several authors have recently reported predictions for γ -jet in heavy-ion collisions [47–50]. As a demonstration of how such calculations can be compared to the data, the I_{AA} values as a function of z_T are compared to energy loss predictions [50] in Fig. 8. The calculation uses effective fragmentation functions to parametrize the average energy loss of the leading parton by gluon radiation in terms of a parameter ϵ_0 that is expected to be proportional to the initial gluon density [51]. As in most energy loss calculations, the energy loss of subleading partons and possible medium response effects are neglected. We note that both of these may be important at low values of z . The data are well reproduced by the model over the range of values of ϵ_0 provided, 1.48–1.88 GeV/fm. This corresponds roughly to the range of ϵ_0 allowed by comparison to the PHENIX $\pi^0 R_{AA}$ data of $1.9_{-0.5}^{+0.2}$ [52].

²See Equation 1 in Ref. [51].

It should be noted that the calculation rejects fragmentation photons with an isolation cut. Such a procedure has not yet been demonstrated in central Au + Au data, although doing so would help to eliminate beyond-leading-order effects.

VI. CONCLUSIONS

We have presented the first direct γ -h measurements in Au + Au and $p + p$ collisions at the Relativistic Heavy Ion Collider (RHIC). A significant suppression of $I_{AA} = 0.32 \pm 0.12^{\text{stat}} \pm 0.09^{\text{sys}}$ for the away-side charged hadron yield in the range $3 < p_T^h < 5 \text{ GeV}/c$ is observed for direct photon triggers in Au + Au as compared to $p + p$. Furthermore, the level of suppression is found to be consistent with the single-particle suppression rate and the importance of energy-loss geometry, notably the expectation of surface emission in the kinematic range sampled. A possible indication that energy-loss geometry may also be important in dijet suppression is that γ -h suppression I_{AA} is also observed to be quite similar to that of dihadron suppression in central events; however, the current precision of the data does not exclude substantial differences. In the $p + p$ data z_T scaling is observed, suggesting that the measured z_T distribution (Fig. 7) is a statistically acceptable representation of the fragmentation function of the quark jet recoiling away from the direct photon. Improvement of the statistical and systematic precision of the measurements should allow further tests of vacuum fragmentation expectations in $p + p$ collisions and insights into details of the medium modification of jet fragmentation in Au + Au. Such studies have begun using subsequently collected larger data sets. The projected order of magnitude increase in RHIC luminosity over the next few years will enable true precision measurements.

ACKNOWLEDGMENTS

We thank the staff of the Collider-Accelerator and Physics Departments at Brookhaven National Laboratory and the staff of the other PHENIX participating institutions for their vital contributions. We acknowledge support from the Office of Nuclear Physics in the Office of Science of the Department of Energy, the National Science Foundation, a sponsored research grant from Renaissance Technologies LLC, Abilene Christian University Research Council, Research Foundation of SUNY, and Dean of the College of Arts and Sciences, Vanderbilt University (USA), Ministry of Education, Culture, Sports, Science, and Technology and the Japan Society for the Promotion of Science (Japan), Conselho Nacional de Desenvolvimento Científico e Tecnológico and Fundação de Amparo à Pesquisa do Estado de São Paulo (Brazil), Natural Science Foundation of China (People's Republic of China), Ministry of Education, Youth and Sports (Czech Republic), Centre National de la Recherche Scientifique, Commissariat à l'Énergie Atomique, and Institut National de Physique Nucléaire et de Physique des Particules (France), Ministry of Industry, Science and Technologies, Bundesministerium für Bildung und Forschung, Deutscher Akademischer Austausch Dienst, and Alexander von Humboldt Stiftung (Germany), Hungarian National Science Fund, OTKA (Hungary), Department of Atomic Energy (India), Israel Science Foundation (Israel), Korea Research Foundation and Korea Science and Engineering Foundation (Korea), Ministry of Education and Science, Russia Academy of Sciences, Federal Agency of Atomic Energy (Russia), VR and the Wallenberg Foundation (Sweden), the US Civilian Research and Development Foundation for the Independent States of the Former Soviet Union, the US-Hungarian Fulbright Foundation for Educational Exchange, and the US-Israel Binational Science Foundation.

-
- [1] K. Adcox *et al.* (PHENIX Collaboration), Nucl. Phys. **A757**, 184 (2005).
 - [2] A. Adare *et al.* (PHENIX Collaboration), Phys. Rev. Lett. **101**, 232301 (2008).
 - [3] B. Muller and J. L. Nagle, Annu. Rev. Nucl. Part. Sci. **56**, 93 (2006).
 - [4] A. Adare *et al.* (PHENIX Collaboration), Phys. Rev. C **78**, 014901 (2008).
 - [5] B. Muller, Phys. Rev. C **67**, 061901(R) (2003).
 - [6] T. Renk, Phys. Rev. C **78**, 014903 (2008).
 - [7] K. J. Eskola, H. Honkanen, C. A. Salgado, and U. A. Wiedemann, Nucl. Phys. **A747**, 511 (2005).
 - [8] C. Loizides, Eur. Phys. J. C **49**, 339 (2007).
 - [9] T. Renk and K. J. Eskola, Phys. Rev. C **75**, 054910 (2007).
 - [10] H.-z. Zhang, J. F. Owens, E. Wang, and X. N. Wang, J. Phys. G **35**, 104067 (2008).
 - [11] A. Drees, H. Feng, and J. Jia, Phys. Rev. C **71**, 034909 (2005).
 - [12] S. S. Adler *et al.* (PHENIX Collaboration), Phys. Rev. Lett. **94**, 232301 (2005).
 - [13] X.-N. Wang and Z. Huang, Phys. Rev. C **55**, 3047 (1997).
 - [14] X.-N. Wang, Z. Huang, and I. Sarcevic, Phys. Rev. Lett. **77**, 231 (1996).
 - [15] J. F. Owens, Rev. Mod. Phys. **59**, 465 (1987).
 - [16] T. Ferbel and W. R. Molzon, Rev. Mod. Phys. **56**, 181 (1984).
 - [17] W. Vogelsang and M. R. Whalley, J. Phys. G **23**, A1 (1997).
 - [18] K. Adcox *et al.* (PHENIX Collaboration), Nucl. Instrum. Methods A **499**, 469 (2003).
 - [19] M. Allen *et al.* (PHENIX Collaboration), Nucl. Instrum. Methods A **499**, 549 (2003).
 - [20] S. S. Adler *et al.* (PHENIX Collaboration), Phys. Rev. Lett. **91**, 241803 (2003).
 - [21] K. Adcox *et al.* (PHENIX Collaboration), Nucl. Instrum. Methods A **499**, 489 (2003).
 - [22] L. Aphecetche *et al.* (PHENIX Collaboration), Nucl. Instrum. Methods A **499**, 521 (2003).
 - [23] S. S. Adler *et al.* (PHENIX Collaboration), Phys. Rev. C **76**, 034904 (2007).
 - [24] S. S. Adler *et al.* (PHENIX Collaboration), Phys. Rev. C **75**, 024909 (2007).
 - [25] K. Adcox *et al.* (PHENIX Collaboration), Nucl. Instrum. Methods A **499**, 489 (2003).
 - [26] S. Afanasiev *et al.* (PHENIX Collaboration), arXiv:0903.4886 [nucl-ex].
 - [27] S. S. Adler *et al.* (PHENIX Collaboration), Phys. Rev. Lett. **96**, 032302 (2006).
 - [28] S. S. Adler *et al.* (PHENIX Collaboration), Phys. Rev. C **71**, 051902 (2005).

- [29] M. McCumber and J. Frantz, *Acta Phys. Hung. A* **27**, 213 (2006).
- [30] S. S. Adler *et al.* (PHENIX Collaboration), *Phys. Rev. Lett.* **97**, 052301 (2006).
- [31] S. S. Adler *et al.* (PHENIX Collaboration), *Phys. Rev. Lett.* **91**, 182301 (2003).
- [32] A. Adare *et al.* (PHENIX Collaboration) (to be published).
- [33] K. Miki (PHENIX Collaboration), *J. Phys. G* **35**, 104122 (2008).
- [34] S. Huang (PHENIX Collaboration), *J. Phys. G* **35**, 104105 (2008).
- [35] S. S. Adler *et al.* (PHENIX Collaboration), *Phys. Rev. Lett.* **98**, 012002 (2007).
- [36] T. Isobe, *Nucl. Phys. A* **783**, 569 (2007).
- [37] T. Isobe (PHENIX Collaboration), *J. Phys. G* **34**, S1015 (2007).
- [38] A. Adare *et al.* (PHENIX Collaboration), *Phys. Rev. D* **76**, 051106 (2007).
- [39] S. S. Adler *et al.* (PHENIX Collaboration), *Phys. Rev. C* **77**, 014905 (2008).
- [40] S. S. Adler *et al.* (PHENIX Collaboration), *Phys. Rev. C* **69**, 034910 (2004).
- [41] S. S. Adler *et al.* (PHENIX Collaboration), *Phys. Rev. Lett.* **95**, 202001 (2005).
- [42] S. S. Adler *et al.* (PHENIX Collaboration), *Phys. Rev. D* **74**, 072002 (2006).
- [43] M. Della Negra *et al.* (CCHK), *Nucl. Phys.* **B127**, 1 (1977).
- [44] R. P. Feynman, R. D. Field, and G. C. Fox, *Nucl. Phys.* **B128**, 1 (1977).
- [45] A. Kulesza, G. Sterman, and W. Vogelsang, *Nucl. Phys.* **A721**, 591 (2003).
- [46] P. Aurenche, J. P. Guillet, E. Pilon, M. Werlen, and M. Fontannaz, *Phys. Rev. D* **73**, 094007 (2006).
- [47] F. Arleo, *J. High Energy Phys.* 09 (2006) 015.
- [48] T. Renk, *Phys. Rev. C* **74**, 034906 (2006).
- [49] G. Y. Qin, J. Ruppert, C. Gale, S. Jeon, and G. D. Moore, *Eur. Phys. J. C* **61**, 819 (2009).
- [50] H. Zhang, J. F. Owens, E. Wang, and X.-N. Wang, arXiv:0902.4000 [nucl-th] (private communication).
- [51] H. Zhang, J. F. Owens, E. Wang, and X.-N. Wang, *Phys. Rev. Lett.* **98**, 212301 (2007).
- [52] A. Adare *et al.* (PHENIX Collaboration), *Phys. Rev. C* **77**, 064907 (2008).